Molecular and Cellular Endocrinology 610 (2025) 112668

Contents lists available at ScienceDirect

Molecular and Cellular Endocrinology

journal homepage: www.elsevier.com/locate/mce

OXTR overexpression induces polycystic ovary syndrome-like phenotype via prolactin/p-STAT3 signaling in mice

Shuilian Wang [a,1], Xinyue Bao [a,1], Ziying Liu [a], Mingjun San [b], Lingyu Zhang [a], Yanjun Liu [a], Mingyan Yang [a], Yaowu Zheng [b,*], Dan Li [a,**]

[a] School of Basic Medicine, Liaoning Province Key Laboratory for Phenomics of Human Ethnic Specificity and Critical Illness (LPKL-PHESCI), Shenyang Medical College, Shenyang, Liaoning, 110034, China
[b] Transgenic Research Center, Northeast Normal University, Changchun, Jilin, 130024, China

ARTICLE INFO

Keywords:
Oxtr
Polycystic ovary syndrome
Follicular development
Hyperprolactinemia

ABSTRACT

Polycystic ovary syndrome (PCOS), a prevalent endocrine disorder, represents the most common cause of anovulatory infertility. While the oxytocin receptor (OXTR) is well-characterized in parturition and lactation, its role in follicular development remains undefined. In this study, we establish that global OXTR overexpression in female mice ($^{++}$*Oxtr*) recapitulates cardinal PCOS features, including hyperandrogenism, oligo-ovulation, and polycystic ovarian changes. $^{++}$*Oxtr* females exhibited distinct ovarian pathology marked by follicular atresia, cystic changes, hemorrhage, and deficient corpus luteum formation. These morphological alterations coincided with profound endocrine dysregulation, featuring hyperprolactinemia, suppressed luteinizing hormone (LH) secretion, and progesterone (P) deficiency, contrasting with preserved fertility in $^{++}$*Oxtr* males. Mechanistically, we identified an OXTR-prolactin (PRL)-p-STAT3 axis as central to PCOS pathogenesis. Corresponding to hyperprolactinemia, persistent activation of nuclear p-STAT3 (Tyr705) in $^{++}$*Oxtr* ovaries - absent in WT controls at pregnancy - upregulated folliculogenesis genes (*Lhcgr*, *Pgr*, *Leptin*, *Cyp17a1*) while impairing ovulation. Therapeutic intervention with bromocriptine normalized prolactin and progesterone levels, partially restoring ovarian function. Notably, $^{++}$*Oxtr* females developed metabolic dysfunction characterized by insulin resistance and gonadal adiposity despite maintaining lean phenotypes. Our findings position OXTR as a novel upstream regulator of PCOS pathogenesis with hyperprolactinemia, suggesting bromocriptine may have therapeutic value in hyperprolactinemic PCOS cases. These insights open new avenues for targeted PCOS interventions.

1. Introduction

Polycystic ovary syndrome (PCOS) is a prevalent endocrine-metabolic disorder affecting 5–20 % of women worldwide (Dumesic et al., 2015; Li et al., 2013). This clinically heterogeneous condition is characterized by concurrent reproductive and metabolic dysfunction. Key reproductive features include ovulatory dysfunction, hyperandrogenism, and altered LH/follicle-stimulating hormone (FSH) ratios (Azziz et al., 2016; Diamanti-Kandarakis et al., 2005; Goodarzi and Azziz, 2006), while metabolic disturbances involve central adiposity, insulin resistance, dyslipidemia, and non-alcoholic fatty liver disease (E. B et al., 2018; Burger, 2002; T et al., 2004; W and Y, 2021). These abnormalities collectively increase risks of cardiovascular disease, type 2 diabetes (Ma et al., 2019), and metabolic syndrome (Cj and N, 2019), significantly compromising long-term health outcomes (Fauser et al., 2012). The diagnosis of PCOS requires three criteria: oligo-ovulation or anovulation, clinical manifestations of hyperandrogenism, and polycystic ovarian morphology as evidenced by ultrasound examination (Edinoff et al., 2021). Present in approximately 30 % of PCOS cases (L et al., 2023), hyperprolactinemia also impairs fertility through direct suppression of the hypothalamic-pituitary-gonadal (HPG) axis. Elevated prolactin levels inhibit anterior pituitary release of both LH and FSH, creating a hypogonadotropic state. This hormonal disruption manifests clinically as menstrual irregularities, hypoestrogenism due to impaired follicular development, and ultimately anovulatory infertility (Ub, 2012).

* Corresponding author.
** Corresponding author.
E-mail addresses: zhengyw442@nenu.edu.cn (Y. Zheng), lidan0519@symc.edu.cn (D. Li).
[1] These authors contributed equally: Shuilian Wang and Xinyue Bao.

https://doi.org/10.1016/j.mce.2025.112668
Received 31 July 2025; Received in revised form 22 September 2025; Accepted 25 September 2025
Available online 26 September 2025

The oxytocin receptor (OXTR), a G protein-coupled receptor expressed in reproductive tissues (uterus, mammary glands, ovaries) and brain regions (limbic system, hypothalamus, cortex) (Amin et al., 2023; Hidema et al., 2016), mediates both central neuromodulation and peripheral endocrine functions via hypothalamic oxytocin neurons (Gimpl and Fahrenholz, 2001). Beyond reproduction, OXTR modulates social behavior, stress responses, and metabolic homeostasis (Kasahara et al., 2013; Kosfeld et al., 2005; Neumann, 2002). Its crucial reproductive roles include facilitating parturition through uterine contractions and lactation via mammary myoepithelial cell stimulation (Fuchs et al., 1995; Iovino et al., 2021; Russell et al., 2003). Our previous studies demonstrate that OXTR overexpression in female mice causes pathological outcomes: impaired mammary development, complete lactation failure (100 % offspring mortality) (Li et al., 2018), and spontaneous HER2-positive mammary tumorigenesis (Li et al., 2021). Although OXTR's contractile function in parturition and lactation is well-characterized (Hasan, 2024), its role in ovarian physiology remains unclear. Here, we investigated OXTR's regulation of follicular development and its potential contribution to polycystic ovary pathogenesis.

2. Materials and methods

2.1. Materials and reagents

All chemicals and reagents were obtained from Sigma (USA), Vazyme and Takara (China).

2.2. Animals

All animal experiments were approved by the Shenyang Medical College Ethics Committee (Approval No. SYYXY2023061002). We used β-actin-*Oxtr* transgenic mice (C57BL/6J strain) (MGI:6314370) (Li et al., 2018, 2021) with wild-type (WT) littermates as controls. Experimental animals were housed under specific pathogen-free (SPF) conditions (50 ± 20 % humidity, 21 ± 1 °C, 12h light/dark cycle) with ad libitum access to food and water. Health status was monitored twice weekly, and humane endpoints (lethargy or persistent recumbency) were followed by euthanasia via pentobarbital sodium (intraperitoneal injection, 1 %, 10 mg/kg).

2.3. Genotyping

Genomic DNA was extracted from tail biopsies using GNTK buffer (50 mM KCl, 1 M $MgCl_2$, 10 mM Tris-HCl [pH 8.5], 0.01 % gelatin, 0.45 % Nonidet P-40, 0.45 % Tween-20, and 100 mg/mL proteinase K) at 55 °C for ≥15 h (Malumbres et al., 1997), followed by heat inactivation (95 °C, 15 min). PCR amplification was conducted using specific primers (forward: 5′-AATGCCCTGGCTCACAAATAC-3'; reverse: 5′-GGGACAGCT ATGACTGGGAGTAG-3′) targeting the rb_glob_PA terminator region of pCAGGS vector. The PCR protocol consisted of: initial denaturation at 94 °C for 2 min; 30 cycles of denaturation (94 °C, 30 s), annealing (57 °C, 30 s), and extension (72 °C, 1 min); followed by final extension at 72 °C for 10 min. A 456-bp product confirmed $^{++}$*Oxtr* genotype, while no band was detected in WT controls.

2.4. Estrous cycle assessment

Vaginal smears were collected daily over a period of 18 consecutive days to evaluate the timing of first estrus and overall cyclicity. The stage of the estrous cycle was determined by examining vaginal cytology under an inverted microscope.

2.5. Ovulation analysis, zygotes collection and embryo transfer

Embryos were collected after natural mating. The ovulation rate was assessed by counting zygotes at 0.5 days post-coitum. For embryo transfer, six-week-old F1 (B6 × DBA/2) females were superovulated via intraperitoneal injection of 5IU PMSG followed by 5IU hCG 46 h later. After overnight mating with C57BL/6J stud males, zygotes were collected from the oviduct infundibulum in M2 medium, treated with hyaluronidase, and cultured overnight in M16 medium. Embryos were then transferred into the oviducts of pseudopregnant WT and $^{++}$*Oxtr* females, which were prepared by prior mating with vasectomized C57BL/6J/DBA males.

2.6. Histology and immunohistochemistry (IHC) analysis

Ovarian and adipose tissues underwent 24-h fixation in 4 % paraformaldehyde (PFA), then processed through graded ethanol dehydration, paraffin embedding, and sectioned at 5 μm thickness for hematoxylin-eosin (H&E) staining (Marshall and Horobin, 1973). For immunohistochemistry (IHC), antigen retrieval was conducted using EDTA buffer (pH 8.0) at 95 °C for 15 min. Ovary tissue sections were incubated overnight at 4 °C with the following primary antibodies: rabbit anti-phospho-STAT3 (Tyr705) (CST #9751S, 1:50 dilution) or rabbit anti-OXTR (Proteintech #23045-1-AP, 1:400 dilution). After washing, sections were incubated with HRP-conjugated anti-rabbit secondary antibody (CST #8114P) for 30 min at room temperature. Signal detection used 3,3′-diaminobenzidine (DAB) substrate, followed by hematoxylin nuclear counterstaining. Images were acquired using an Olympus IX71 microscope.

2.7. RNA sequencing (RNA-seq) and analysis

Ovarian tissue RNA from WT and $^{++}$*Oxtr* females was sequenced using Illumina HiSeq 2500. Differentially expressed genes (DEGs) were identified with thresholds of $Q < 0.05$ and $|\log2FC|>1$, followed by functional enrichment analysis (FDR correction, $q < 0.05$). Data visualization utilized specialized bioinformatics tools, and key DEGs were validated by quantitative real-time PCR (RT-PCR). All samples were processed in parallel to minimize batch effects.

2.8. Quantitative real-time PCR (RT-PCR)

Total RNA was extracted from mouse ovarian tissues using TRIzol reagent (Takara). cDNA was synthesized from 1 μg RNA using the PrimeScript™ cDNA Synthesis Kit (Takara) according to the manufacturer's instructions. RT-PCR was performed using SYBR Green Master Mix (Takara) under standard cycling conditions. Relative gene expression was calculated by the $2^{-\Delta\Delta CT}$ method, and normalized to 18S ribosomal RNA. Primer sequences are provided in Supplementary Table S1.

2.9. Western blot assay

Mouse ovarian tissues were homogenized in RIPA lysis buffer. Total protein (40 μg) was separated by 10 % SDS-PAGE and transferred to PVDF membranes. The membranes were incubated overnight at 4 °C with primary antibodies: rabbit anti-OXTR (ab181077; 1:5,000 dilution) and rabbit anti-GAPDH (AP0063, Bioworld; 1:10,000 dilution). After three TBST washes, the membranes were incubated for 1 h at room temperature with HRP-conjugated secondary antibodies: donkey anti-rabbit IgG (GE Healthcare; 1:3,000 dilution). Protein bands were visualized using Amersham™ ECL™ reagent (GE Healthcare), with GAPDH serving as a loading control.

2.10. ELISA assay

Serum samples were obtained and clotted for 30 min at room temperature before centrifugation (400×*g*). Mouse serum testosterone (DEMEDITEC Diagnostics GmbH, DEV9911), luteinizing hormone (LH, CUSABIO, CSB-E12770m), progesterone (DEMEDITEC Diagnostics

GmbH, DEV9988), estradiol (Enzo, Cat ADI-900-174) and prolactin (Abcam, AB100736) levels were measured using commercial ELISA kits according to manufacturers' instructions, with detection limits of 0.024 ng/ml, 0.5mIU/ml, 0.04 ng/mL, 14 pg/mL, and 30 pg/mL. Absorbance was measured using a SpectraMax microplate reader (Molecular Devices).

2.11. Glucose and insulin tolerance test

For the intraperitoneal glucose tolerance test (IPGTT), 9-week-old females were fasted for 16 h with free access to water before receiving an intraperitoneal injection of glucose (2 g/kg). Blood glucose levels were measured from the tail vein at 0, 30, 60, 90 and 120 min using a glucometer (Omron).

For the intraperitoneal insulin tolerance test (IPITT), 9-week-old females were fasted for 4 h with water available ad libitum. After intraperitoneal insulin injection (0.75 U/kg), tail blood glucose was assessed at 0, 30, 60, 90, and 120 min using a glucometer (Omron).

2.12. CUT&Tag

Following euthanasia, ovaries were immediately dissected and homogenized for nuclear extracts using a Nuclear Extraction Kit (SN0020, Solarbio). The CUT&Tag procedure (Vazyme, TD904-C2) began with nuclei incubation using ConA Beads Pro (10 min, RT), followed by centrifugation and supernatant removal. Nuclear-bead complexes were

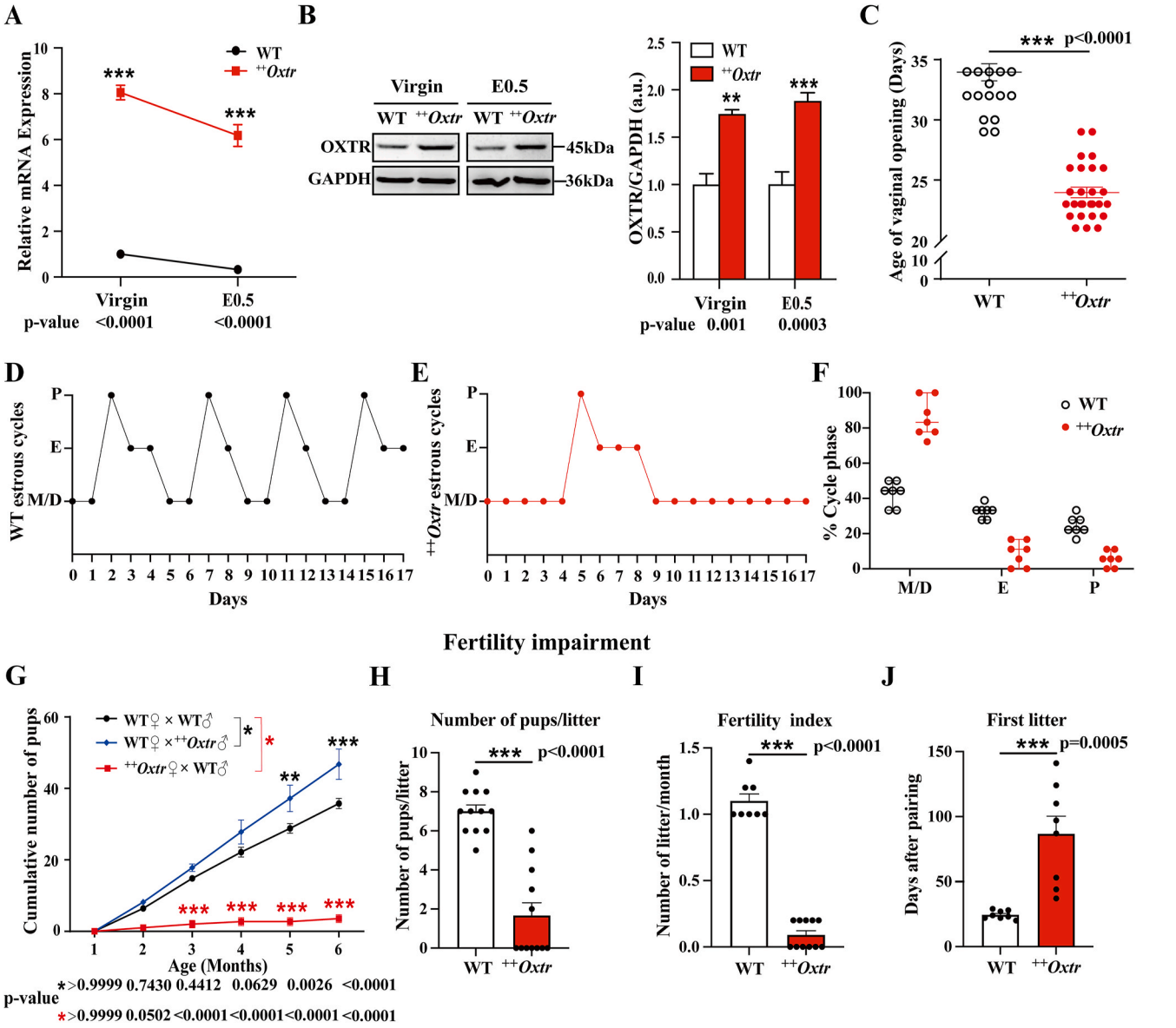

Fig. 1. ++*Oxtr* females exhibit reproductive impairment. (A) *Oxtr* mRNA expression in virgin and E0.5 (Embryo 0.5 days) ovaries by RT-PCR, n = 3/group. (B) OXTR protein levels in virgin and E0.5 ovaries by Immunoblotting. GAPDH is served as a loading control. Protein quantifications using Image J, n = 3/group. (C) Age of first vaginal opening in females (indicating puberty onset). WT, n = 15; ++*Oxtr*, n = 27. (D–E) Representative estrous cycle profiles of WT (D) and ++*Oxtr* (E) females over 18 consecutive days. M/D: metestrus/diestrus; E: estrus; P: proestrus. (F) Quantitative analysis of estrous cyclicity. Scatter plot showing the percentage of time spent in each phase of the estrous cycle by WT and ++*Oxtr* females (n = 7/group). Horizontal lines represent medians; vertical bars indicate interquartile ranges (25th-75th percentiles). (G) Cumulative pup numbers over 5 months of pairing from WT pairs, ++*Oxtr* males mated with WT females, ++*Oxtr* females mated with WT males. n = 6 cages/group. (H) Number of pups per litter, n = 12 litters/group. (I) Fertility index: Number of litters/month. WT, n = 8; ++*Oxtr*, n = 11. (J) Days to first litter post-pairing, n = 8 litters/group. Data were represented as mean ± SEM. **p < 0.01, ***p < 0.001, calculated with one-way ANOVA (≥3 groups) or unpaired two-tailed t-tests (2 groups).

resuspended in 50 μL chilled Antibody Buffer containing either anti-H3K4me3 (CST #9145T; 1:50) or anti-p-STAT3 (CST #9751S; 1:100) primary antibodies with gentle inversion mixing, then incubated overnight at 4 °C. After secondary antibody incubation (goat anti-rabbit/mouse IgG, 1:100; 1h, RT) and washing, tagmentation was performed using pA/G-Tnp Pro (1h, 37 °C) followed by DNA extraction, library amplification, and purification (Vazyme N411).

2.13. Bromocriptine treatment

Bromocriptine (Sigma) was prepared as a 1 mg/mL solution in sterile saline (0.9 % NaCl). Mice received daily subcutaneous injections of 200 μg bromocriptine for 30 days. Control WT and $^{++}$*Oxtr* females received equivalent saline treatments.

2.14. Statistical analysis

All data are presented as mean ± standard error of the mean (SEM). Statistical comparisons were performed using GraphPad Prism 10, with one-way ANOVA (≥3 groups) or unpaired two-tailed t-tests (two groups). Significance thresholds were set at *p < 0.05, **p < 0.01, and ***p < 0.001.

3. Results

3.1. $^{++}$*Oxtr females develop reproductive disorders*

To explore the role of OXTR in reproduction, we used transgenic mice with universal overexpression of OXTR driven by the β-actin promoter ($^{++}$*Oxtr*), as previously described (Li et al., 2018, 2021). *Oxtr* overexpression was confirmed in the brain, hypothalamus, and mammary gland (Fig. S1A). Additionally, RT-PCR, immunoblotting and immunostaining validated OXTR overexpression in ovary (Fig. 1A and B and S1B). $^{++}$*Oxtr* females exhibited earlier puberty onset than WT, with vaginal opening at 3 weeks (Fig. 1C). Estrous cycles were monitored over 18 days. $^{++}$*Oxtr* females exhibited significant disrupted cycles,

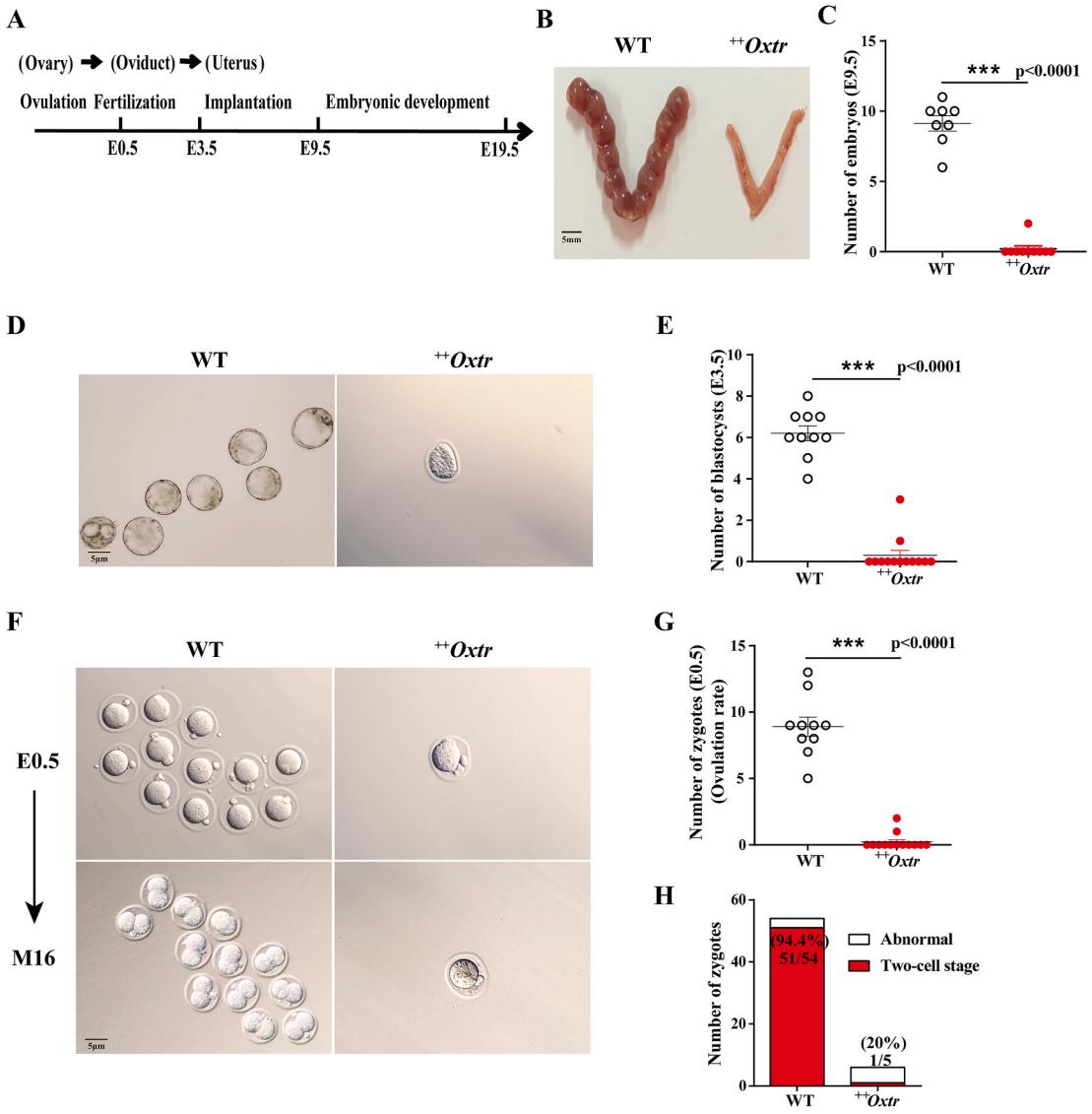

Fig. 2. Reproductive analysis during pregnancy. (A) Timeline for reproduction and embryo retrieval during pregnancy. (B) Representative E9.5 uterine embryos from 12-week-old WT and $^{++}$*Oxtr* females. Scale bar: 5 mm. (C) Uterine embryo counts at E9.5. WT, n = 8; $^{++}$*Oxtr*, n = 10. (D) Representative E3.5 uterine blastocysts from 12-week-old WT and $^{++}$*Oxtr* females. Scale bar: 5 μm. (E) Normal blastocyst counts in uterines at E3.5. WT, n = 10; $^{++}$*Oxtr*, n = 13. (F) Representation of zygotes and 2-cell embryos after 24h culture in M16 medium from E0.5 WT and $^{++}$*Oxtr* females. Scale bar: 5 μm. (G) Oviductal zygote counts at E0.5 serve as a proxy for ovulation rate. WT, n = 10; $^{++}$*Oxtr*, n = 13. (H) Zygote-to-2-cell transition rates, n = 5/group. Data were represented as mean ± SEM. ***p < 0.001, calculated with unpaired two-tailed t-tests (two groups).

characterized by prolonged metestrus and diestrus phases compared to WT (Fig. 1D–F). During a 5-month breeding period, $^{++}$*Oxtr* females also showed diminished fertility and fecundity, as indicated by fewer pups (Fig. 1G and H) and fewer litters (Fig. 1I) produced, along with a significant delay in their first litter (Fig. 1J). In contrast, $^{++}$*Oxtr* males maintained normal fertility, when mated with WT females (Fig. 1G). Thus, $^{++}$*Oxtr* females, but not males, exhibit reproductive impairment.

3.2. $^{++}$*Oxtr females fail to release normal eggs*

The reproductive process includes ovulation, fertilization in the oviduct (Embryo 0.5 day, E0.5), embryo transit to the uterus, blastocyst formation and implantation (E3.5), followed by rapid embryonic growth (E9.5) and birth at 19.5–20.5 days (Fig. 2A). By E9.5, nearly no embryos were present in $^{++}$*Oxtr* uteri (Fig. 2B and C). Similarly, at E3.5, $^{++}$*Oxtr* uteri contained very few normal blastocysts (Fig. 2D and E). At E0.5, $^{++}$*Oxtr* oviducts had almost no viable zygotes, indicating a reduced ovulation rate. When zygotes from $^{++}$*Oxtr* females were extracted and cultured in vitro, they were fewer in number, lower in quality compared to WT eggs, with most failing to progress to the two-cell stage after 24 h (Fig. 2F–H). In summary, $^{++}$*Oxtr* females fail to release normal eggs, leading to reproductive impairment.

To assess post-ovulatory stages, we transferred WT embryos into the oviducts of $^{++}$*Oxtr* and WT females at E0.5 (Fig. 3A). After embryos transfer (ET), $^{++}$*Oxtr* uteri contained normal blastocysts at rates comparable to WT (Fig. 3B–D), confirming successful embryo transit and implantation. Offspring gains from $^{++}$*Oxtr* females suggested normal embryonic development after ET (Fig. 3E). Overall, aside from defective ovulation, $^{++}$*Oxtr* females show no other reproductive abnormalities.

3.3. *OXTR overexpression induces a PCOS-like phenotype*

To further investigate the oligo-ovulatory phenotype in $^{++}$*Oxtr* females, we analyzed ovarian development. $^{++}$*Oxtr* females displayed significant reduced ovary weight (Fig. 4A), and ovarian hemorrhage was observed in 79.2 % of $^{++}$*Oxtr* females (Fig. 4B and C). Ovarian histological analysis pointed to the abnormal follicle development in $^{++}$*Oxtr* females, characterized by more atretic/immature cystic follicles and the presence of fewer post-ovulation corpora lutea than WT, resembling polycystic ovarian changes (Fig. 4D). Serum hormone analysis showed elevated testosterone (Fig. 4E) but reduced LH and progesterone (P) (Fig. 4F and G) in $^{++}$*Oxtr* females during diestrus, with no difference in estradiol (Fig. 4H). RNA sequencing (RNA-seq) identified 250 differentially expressed genes (DEGs) of $^{++}$*Oxtr* against WT ovaries (Fig. S2), 84 of which (33.6 %) overlapped with PCOS-related genes linked to PPAR, hormonal, and metabolic pathways (Fig. 4I). We then checked whether $^{++}$*Oxtr* females presented PCOS-like metabolic alterations. $^{++}$*Oxtr* females had lower body weight (Fig. 4J), but increased gonadal white adipose tissue (gWAT) mass (Fig. 4K), gWAT whitening (Fig. 4L), and reduced insulin sensitivity compared with WT (Fig. 4M). In contrast, $^{++}$*Oxtr* and WT females showed comparable glucose tolerance in IPGTT tests (Fig. S3). Together, these findings align with key PCOS diagnostic criteria: hyperandrogenism, oligo-anovulation, and polycystic ovarian changes.

3.4. *OXTR overexpression leads to activation of prolactin (PRL)/p-STAT3 pathway*

Using the Cistrome database, we predicted OXTR-associated transcription factors (TFs) and constructed a regulatory network, identifying 63 transcription factors, which were visualized using Cytoscape (Fig. 5A). KEGG analysis of 63 TFs highlighted the prolactin signaling pathway (Fig. 5B). When comparing the overlap of prolactin signaling, OXTR-related transcription factors, with PCOS genes, 3 transcription factors STAT3, ESR1 and RELA were identified (Fig. 5C). Prolactin was maintained at higher level in both virgin and E0.5 $^{++}$*Oxtr* females (Fig. 5D). Corresponding to the high prolactin, total *Stat3* mRNA in $^{++}$*Oxtr* ovary was higher than WT (Fig. 5E). Notably, nuclear p-STAT3 (Tyr705), nearly absent in WT ovaries, remained activated in $^{++}$*Oxtr* ovaries until pregnancy (Fig. 5F). CUT&Tag analysis revealed p-STAT3 and H3K4me3 targets. Key hormone receptors and follicular development genes, including *Lhcgr*, *Pgr*, *Leptin*, *Retn*, *Mc2r*, *Acvr1c*, *Cyp2e1*, *Cyp27a1*, *Cyp17a1*, *Cyp26b1*, *Ucp3*, *Dcn* and *Lox* were up-regulated in $^{++}$*Oxtr* ovaries (Fig. 5G–I), with strong p-STAT3 and H3K4me3 enrichment (Fig. 5J). Hormone receptors, *Fshr*, *Esr1* and *Ar* expression remained unaffected (Fig. 5G). These results suggest PRL/p-STAT3 pathway activation in OXTR-driven PCOS.

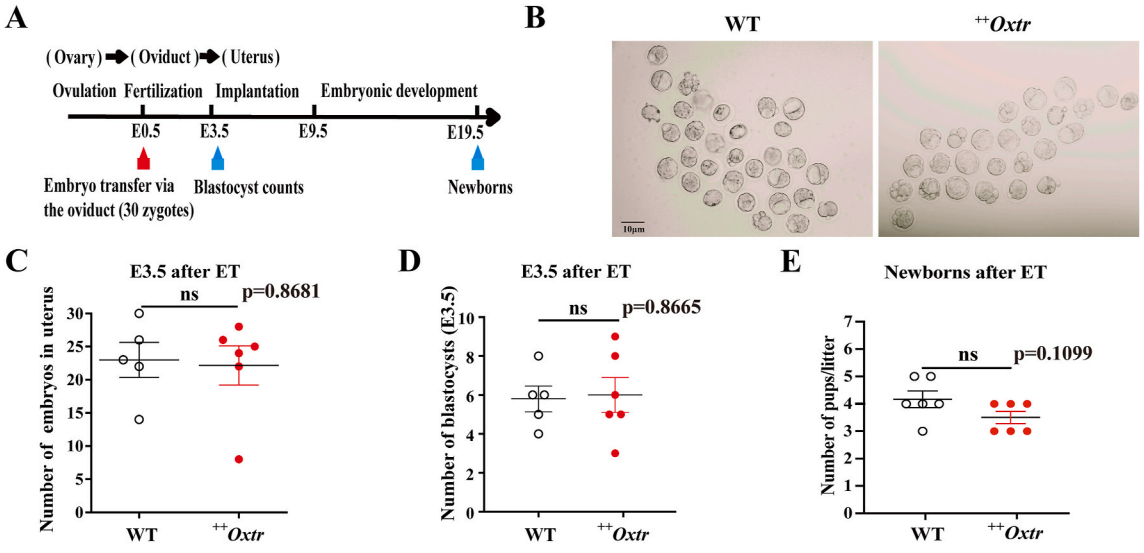

Fig. 3. Reproductive analysis of females after WT embryos transfer (ET). (A) Timeline for reproduction and embryo transfer during pregnancy. (B) Representative E3.5 uterine embryos post- ET. Scale bar: 10 μm. (C) Uterine embryo counts at E3.5 post-ET. WT, n = 5; $^{++}$*Oxtr*, n = 6. (D) Normal blastocyst counts in uterines at E3.5 post-ET. WT, n = 5; $^{++}$*Oxtr*, n = 6. (E) Newborns/litter post-ET, n = 6/group. Data were represented as mean ± SEM, ns means no significance, calculated with unpaired two-tailed t-tests (two groups).

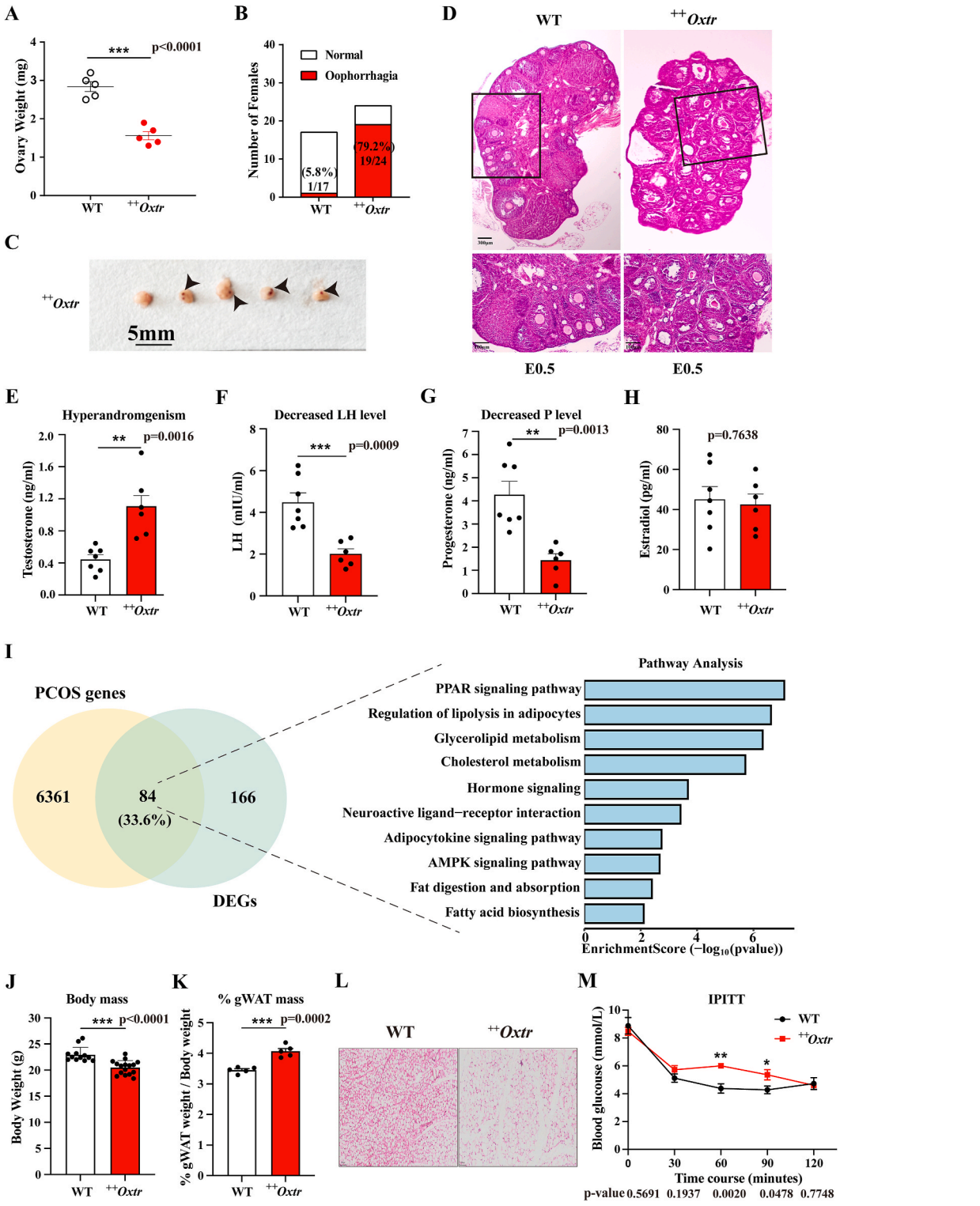

Fig. 4. OXTR overexpression induces a PCOS-like phenotype. (A) Ovarian weight in 12-week-old virgin WT and $^{++}$*Oxtr* females, n = 5/group. (B) Incidence of ovarian hemorrhage. WT, n = 17; $^{++}$*Oxtr*, n = 24. (C) Representative hemorrhagic ovaries of $^{++}$*Oxtr* females, arrows indicate hemorrhage. Scale bar: 5 mm. (D) Representative images of H&E staining of ovaries from 12-week-old E0.5 WT and $^{++}$*Oxtr* females. Scale bar: 300 μm (upper), 100 μm (lower). (E) Serum testosterone levels of WT and $^{++}$*Oxtr* females in diestrus. WT, n = 7; $^{++}$*Oxtr*, n = 6. (F) Serum LH levels of WT and $^{++}$*Oxtr* females in diestrus. WT, n = 7; $^{++}$*Oxtr*, n = 6. (G) Serum progesterone (P) levels of WT and $^{++}$*Oxtr* females in diestrus. WT, n = 7; $^{++}$*Oxtr*, n = 6. (H) Serum estradiol levels of WT and $^{++}$*Oxtr* females in diestrus. WT, n = 7; $^{++}$*Oxtr*, n = 6. (I) Venn diagram displayed the overlap between PCOS-related genes (Data from GeneCards) and the DEGs in $^{++}$*Oxtr* against WT ovaries. Ontology analysis of overlapping genes. (J) Body weight of 9-week-old WT and $^{++}$*Oxtr* females, WT, n = 12; $^{++}$*Oxtr*, n = 16. (K) Percent gWAT mass normalized to body weight of 9-week-old females, n = 5/group. (L) Representative H&E-stained sections of gWAT from 9-week-old female mice, scale bar: 100 μm. (M) IPITT of 9-week-old females fasted for 4h, n = 5/group. Data were represented as mean ± SEM. *p < 0.05, **p < 0.01, ***p < 0.001, calculated with unpaired two-tailed t-tests (two groups).

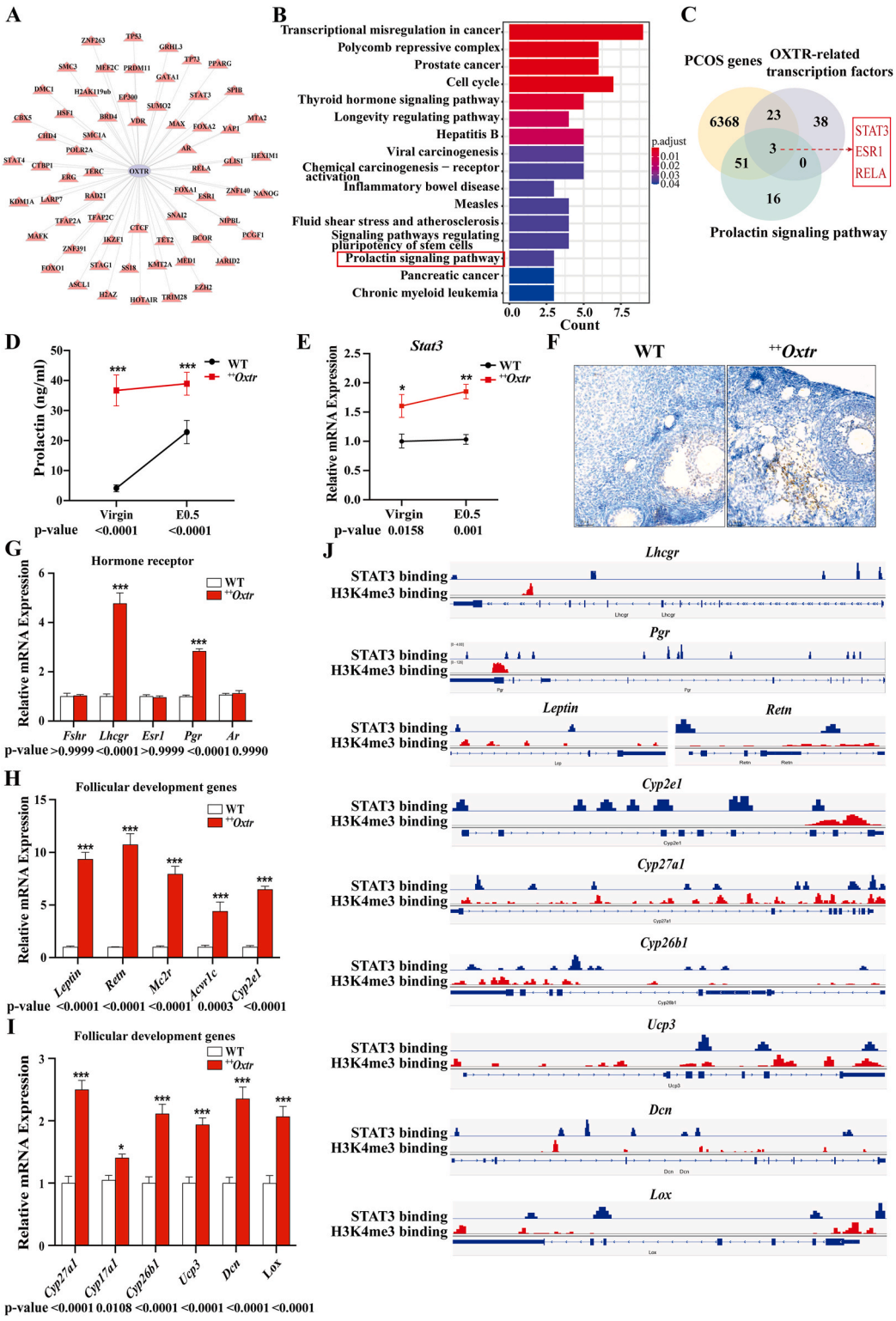

Fig. 5. OXTR overexpression activates PRL/p-STAT3 pathway. (A) OXTR-associated transcriptional network (63 transcription factors, TFs) from Cistrome DB, visualized with Cytoscape. (B) KEGG pathway analysis of OXTR-linked TFs. (C) The overlap between PCOS genes (GeneCards), OXTR TFs, and prolactin signaling identifies STAT3, ESR1, and RELA. (D) Serum prolactin levels of virgin and E0.5 females, n = 4–5/group. (E) Total *Stat3* mRNA expression in virgin and E0.5 ovaries by RT-PCR, n = 3/group. (F) Immunostaining analysis of p-STAT3 in E0.5 WT, and $^{++}$*Oxtr* ovaries. Nuclei were stained blue with hematoxylin. Scale bar: 50 μm. (G) Gene expression of hormone receptor *Fshr*, *Lhcgr*, *Esr1*, *Pgr*, and *Ar* in virgin ovaries by RT-PCR, n = 3/group. (H–I) Gene expression of follicular development genes, including *Leptin*, *Retn*, *Mc2r*, *Acvr1c*, *Cyp2e1*, *Cyp27a1*, *Cyp17a1*, *Cyp26b1*, *Ucp3*, *Dcn* and *Lox* in virgin ovaries by RT-PCR, n = 3/group. (J) CUT&Tag profiles of p-STAT3/H3K4me3 on *Lhcgr, Pgr, Leptin*, *Retn*, *Cyp2e1*, *Cyp27a1*, *Cyp26b1*, *Ucp3*, *Dcn* and *Lox* in virgin WT ovaries. Data were represented as mean ± SEM. *p < 0.05, **p < 0.01, ***p < 0.001, calculated with unpaired two-tailed t-tests (two groups). (For interpretation of the references to colour in this figure legend, the reader is referred to the Web version of this article.)

3.5. Bromocriptine alleviated OXTR-induced abnormal follicular development

To prove that prolactin signaling is mediating OXTR-induced PCOS, prolactin inhibitor bromocriptine (Br, 200ug) was subcutaneously administered daily to $^{++}$*Oxtr* females for 30 days. Among Br targets, 36.9 % (184/499) were PCOS-related (Fig. 6A). Br treatment significantly inhibited serum prolactin level in $^{++}$*Oxtr* females and reversed

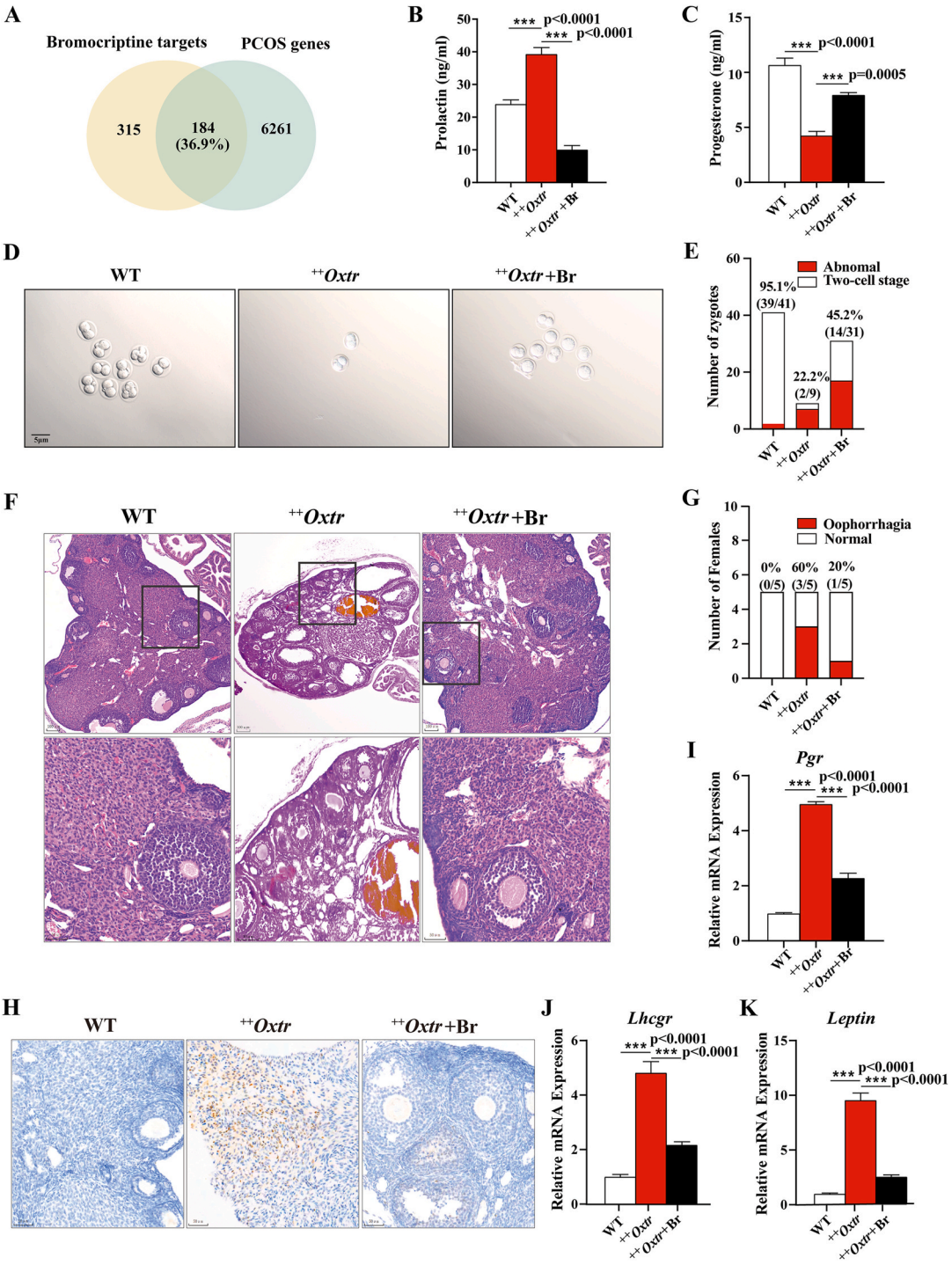

Fig. 6. Bromocriptine alleviates OXTR-induced follicular defects. 12-week-old females received daily bromocriptine (Br; 200 μg in 1 mg/ml solution) or vehicle for 30 days. (A) Venn diagram displayed the overlap between Br targets (Data from Swiss Target Prediction, SuperPred and PharmMapper) and PCOS-related genes (GeneCards). (B) Serum prolactin levels in E0.5 WT, $^{++}$*Oxtr*, and $^{++}$*Oxtr* females with Br treatment, n = 5/group. (C) Serum progesterone levels in E0.5 WT, $^{++}$*Oxtr*, and $^{++}$*Oxtr* females with Br treatment, n = 5/group. (D) Representative 2-cell embryos after 24h culture in M16 medium from E0.5 WT, $^{++}$*Oxtr*, and $^{++}$*Oxtr* females with Br treatment. Scale bar: 5 μm. (E) Zygote-to-two-cell transition rates, n = 5/group. (F) Representative images of H&E staining of E0.5 ovaries. Scale bar: 100 μm (upper), 50 μm (lower). (G) Ovarian hemorrhage incidence, n = 5/group. (H) p-STAT3 immunostaining of ovaries at E0.5. Nuclei were stained blue with hematoxylin. Scale bar: 50 μm. (I–K) Gene expression of *Pgr*, *Lhcgr*, and *Leptin* in E0.5 ovaries by RT-PCR, n = 3/group. Data were represented as mean ± SEM. ***p < 0.001, calculated with one-way analysis of variance (ANOVA). (For interpretation of the references to colour in this figure legend, the reader is referred to the Web version of this article.)

OXTR-induced hyperprolactinemia (Fig. 6B). Low progesterone of $^{++}$*Oxtr* females was relieved (Fig. 6C). Meanwhile, Br increased fertilized egg counts, and improved two-cell embryo development, indicating the oligo-ovulatory phenotype was mitigated (Fig. 6D and E). H&E staining showed fewer atretic follicles, more corpora lutea, and reduced hemorrhage in Br-treated $^{++}$*Oxtr* ovaries, resembling WT morphology (Fig. 6F and G). IHC confirmed p-STAT3 inhibition ((Fig. 6H), and RT-PCR showed downregulation of PRL/p-STAT3 targets (*Pgr*, *Lhcgr*, and *Leptin*) (Fig. 6I–K). Thus, OXTR promotes PCOS via PRL/p-STAT3 signaling.

4. Discussion

Our study demonstrates that global OXTR overexpression in female mice induces a PCOS-like phenotype, characterized by hyperandrogenism, oligo-ovulation, and polycystic ovarian changes. These reproductive defects were driven by aberrant activation of the prolactin (PRL)/p-STAT3 pathway, as evidenced by their reversal following bromocriptine treatment. Specifically, OXTR overexpression triggered prolactin hypersecretion and STAT3 phosphorylation in the ovary, with subsequent nuclear p-STAT3 translocation upregulating follicular development genes. This cascade resulted in impaired folliculogenesis, attenuated preovulatory LH surges, and deficient luteal progesterone production (Fig. 7). Our findings identify OXTR as a novel regulator of ovarian function and reveal a PRL/p-STAT3-dependent mechanism in PCOS pathogenesis.

4.1. The $^{++}$Oxtr females as a novel PCOS model with unique hormonal dysregulation

While OXTR is known to regulate reproductive physiology, including uterine contractility, parturition and lactation, its role in folliculogenesis has been unclear. In contrast to *Oxtr* knockout mice that maintain fertility (Takayanagi et al., 2005), $^{++}$*Oxtr* females exhibited severe reproductive impairment specifically due to abnormal follicular development, featuring increased atretic follicles and decreased corpora lutea - hallmark features of polycystic ovaries. The $^{++}$*Oxtr* phenotype mirrored PCOS diagnostic criteria: hyperandrogenism, oligo-anovulation, and ovarian polycystic changes (T. B et al., 2018; X et al., 2019), supported by transcriptomic evidence of dysregulated hormonal and metabolic pathways, aligning with PCOS genomics (Jx et al., 2018; Mimouni et al., 2021). The observed hormonal profile (marked by hyperprolactinemia, suppressed LH secretion, and progesterone deficiency) reflects disrupted hypothalamic-pituitary-ovarian axis function. Chronic hyperprolactinemia and elevated testosterone synergistically suppress GnRH pulsatility, impairing the preovulatory LH surge and subsequent luteal progesterone production (M and P, 2025). Elevated prolactin levels of $^{++}$*Oxtr* females remain below 50 ng/ml, insufficient to meet pathological prolactinoma. Recent review highlights the potential of AMH as a diagnostic marker for PCOS, emphasizing its correlation with polycystic ovarian morphology and anovulation, its stability across the menstrual cycle, and its ability to reduce interobserver variability compared to ultrasound (Vale-Fernandes et al., 2025c). The ovarian phenotypes observed in $^{++}$*Oxtr* mice are consistent with an AMH-associated PCOS profile. We propose that future studies include AMH in multidimensional phenotypic evaluations to improve diagnostic precision.

Recent study also demonstrated that PCOS and obesity independently and synergistically impair reproductive function, with obesity contributing to insulin resistance and exacerbated hyperandrogenism (Vale-Fernandes et al., 2025b) - patterns also observed in our model. Notably, despite being lean, $^{++}$*Oxtr* females developed insulin resistance and hyperandrogenism, likely due to gonadal adipose dysfunction. We identified 250 differentially expressed genes (DEGs) in $^{++}$*Oxtr* ovaries, 84 of which (33.6 %) overlap known PCOS-related genes involved in PPAR, hormonal, and metabolic pathways. This suggests that OXTR-PRL-p-STAT3-driven hyperprolactinemia may disrupt steroidogenesis and metabolic homeostasis.

4.2. Mechanistic insights: The PRL/p-STAT3 signaling hub

Clinical observations indicate hyperprolactinemia occurs in approximately 30 % of PCOS cases (L et al., 2023) and correlates with metabolic dysfunction (V and T, 2025). Notably, insulin-resistant PCOS patients with lower prolactin demonstrate better responsiveness to metformin treatment (T et al., 2024). Emerging evidence implicates

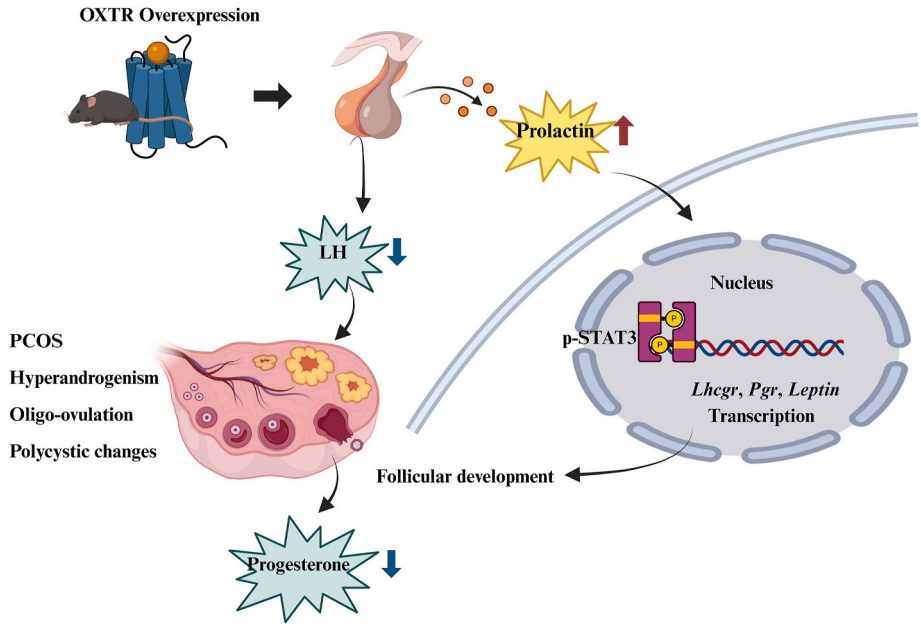

Fig. 7. Role model of OXTR in follicular development. OXTR overexpression in female mice stimulates prolactin hypersecretion, which triggers STAT3 phosphorylation (p-STAT3) and subsequent nuclear translocation. Within the nucleus, p-STAT3 transcriptionally upregulates key folliculogenesis regulators (*Lhcgr*, *Pgr*, and *Leptin*), ultimately inducing a PCOS-like phenotype with attenuated LH surges and luteal progesterone deficiency. This OXTR-PRL-p-STAT3 signaling axis represents a novel mechanistic pathway underlying PCOS-associated ovarian dysfunction.

STAT3, the downstream effector of prolactin signaling, as a central regulator of PCOS pathophysiology (B et al., 2024). While STAT3 ablation in granulosa cells counteracts the therapeutic effects of IL-22 in DHEA-induced PCOS mice (W et al., 2024), pharmacological STAT3 inhibition (via static) improves ovarian function in letrozole-induced PCOS models (Yq et al., 2024). In our study, we observed persistent activation of nuclear p-STAT3 (Tyr705) in $^{++}$*Oxtr* ovaries until pregnancy - a striking contrast to its near absence in pregnant WT ovaries. Integrated bioinformatics and CUT&Tag analyses identified the PRL/p-STAT3 axis as the key mechanistic hub. This pathway directly regulates multiple PCOS-associated genes involved in follicular development, including *Lhcgr*, *Pgr*, *Leptin*, *Lox*, and *Cyp17a1* - all of which were significantly upregulated in $^{++}$*Oxtr* ovaries and showed strong p-STAT3/H3K4me3 binding. Significantly increased LHCGR, LEPIN, LOX and CYP17A were associated with PCOS and anovulation (C et al., 2018; H et al., 2023; L et al., 2025; V et al., 2016). Recent studies have highlighted the role of follicular fluid metabolic and hormonal profiles in PCOS (marked by altered lactate, formate, and citrate levels, along with elevated AMH and reduced progesterone and estradiol), emphasizing mitochondrial and glycolytic dysfunction as key features influencing oocyte quality and fertilization potential (Vale-Fernandes et al., 2025a). These hormonal and metabolic changes mirror the hyperprolactinemia, low progesterone, and ovarian phenotypes in our model. Furthermore, mitochondrial STAT3 dysregulation can drive nuclear p-STAT3 (Tyr705) accumulation to enhance glycolysis, contributing to metabolic dysfunction (Lim et al., 2006; Vaupel et al., 2019). These findings support a mechanism whereby OXTR-mediated hyperprolactinemia and p-STAT3 (Tyr705) activation promote metabolic dysregulation, potentially impairing oocyte quality and fertilization. Our findings demonstrate that OXTR-driven hyperprolactinemia sustains p-STAT3 activation in the ovary, leading to dysregulation of critical folliculogenesis genes and consequent anovulation.

4.3. Therapeutic implications and clinical translation

Bromocriptine, prolactin inhibitor, primarily inhibits prolactin secretion (Zhang et al., 2025). It is generally considered safe for prolonged use, with no significant adverse effects on renal, hepatic, cardiac, or hematologic functions. Commonly reported side effects include transient nausea, headache, and nasal congestion, while serious complications such as myocardial infarction or stroke are rare. Clinically, it is highly effective in restoring fertility by normalizing prolactin levels, supporting ovulation in women, and improving sperm quality in men (Naz et al., 2022). Clinical evidence shows that adding bromocriptine to clomiphene citrate provides no additional benefit over clomiphene alone for ovulation induction or pregnancy outcomes in normoprolactinemic PCOS patients (S et al., 2013). Insulin-resistant PCOS women with lower prolactin levels demonstrate better responses to metformin (T et al., 2024), suggesting prolactin-lowering drugs may be specifically beneficial for hyperprolactinemic PCOS cases. In our study, OXTR overexpression induced a PCOS-like phenotype with hyperprolactinemia. Remarkably, 36.9 % of bromocriptine's molecular targets overlapped with PCOS-associated genes, supporting its potential as a targeted therapy for hyperprolactinemic PCOS subtypes. Bromocriptine can correct HPO axis dysfunction and subsequent improvement in LH release (Liu et al., 2025). In our study, bromocriptine treatment normalized prolactin and progesterone levels while partially restoring ovarian development and ovulation by PRL/p-STAT3 pathway. These findings suggest that bromocriptine shows efficacy in PCOS with elevated prolactin - particularly when combined with metformin - but alternative therapies remain preferable for typical PCOS cases without hyperprolactinemia. Further evaluation of bromocriptine and metformin combination therapy in high-prolactin PCOS is warranted.

4.4. Limitations and future directions

While our model recapitulates key PCOS features, species-specific differences in OXTR signaling warrant caution in human extrapolation. Our previous work established that OXTR overexpression in female mice induced impaired mammary gland development (Li et al., 2018), and spontaneous HER2-positive mammary tumorigenesis (Li et al., 2021), phenotypes associated with $^{++}$*Oxtr* female infertility. Given that prolonged infertility increases breast cancer risk in women (Allen-Brady et al., 2025), the OXTR-driven hormonal disruptions collectively explain the female-specific pathological manifestations. In contrast, OXTR enhances adipocyte browning and improves energy metabolism in males without detrimental effects (Bao et al., 2025). Our study revealed stronger OXTR upregulation in the brain and hypothalamus, with more moderate increase in the ovary. While ovarian OXTR likely acts directly, the predominant central upregulation implies significant involvement of systemic neuroendocrine mechanisms. Tissue-specific genetic models, such as conditional OXTR overexpression in the ovary or hypothalamus, will be essential to dissect these contributions. Future studies should employ purified granulosa cell cultures from $^{++}$*Oxtr* females treated with prolactin or STAT3 inhibitors to clarify the ovarian-specific effects of OXTR activation, independent of central neuroendocrine input. Single-cell analyses could further elucidate cell-type specific responses to OXTR overexpression.

5. Conclusion

We have identified a novel OXTR-PRL-p-STAT3 regulatory axis in follicular development and PCOS-like pathology. These findings expand our understanding of reproductive physiology and suggest new therapeutic strategies for PCOS-associated infertility, particularly in hyperprolactinemic cases.

CRediT authorship contribution statement

Shuilian Wang: Writing – original draft, Methodology, Conceptualization. **Xinyue Bao:** Writing – original draft, Methodology, Conceptualization. **Ziying Liu:** Formal analysis, Data curation. **Mingjun San:** Resources, Methodology. **Lingyu Zhang:** Methodology. **Yanjun Liu:** Methodology. **Mingyan Yang:** Methodology. **Yaowu Zheng:** Writing – review & editing, Conceptualization. **Dan Li:** Writing – review & editing, Methodology, Conceptualization.

Institutional review board statement

All animal studies were reviewed and approved by the Ethics Committee of Shenyang Medical College (Approval No. SYYXY2023061002), conducted in accordance with: the ethical standards stated in the Guidance on the operation of the Animals (Scientific Procedures) and National Institutes of Health's Guide for Care and Use of Laboratory Animals.

Data accessibility

RNA-seq and CUT&Tag datasets are publicly available in the GEO repository (accession numbers: GSE303968 and GSE303969). All data are available from the corresponding author upon reasonable request.

Declaration of competing interest

All authors have reviewed and approved the final manuscript being submitted. The original work is unpublished and not under consideration elsewhere. All authors declare no competing financial interests or personal interests that could influence the work reported in this paper.

Acknowledgements

This work is supported by National Natural Science Foundation of China (82103188), Natural Science Foundation of Liaoning Province, China (2023-MS-325). The above fundings were used for reagents, RNA sequencing and animal maintenance.

Appendix A. Supplementary data

Supplementary data to this article can be found online at https://doi.org/10.1016/j.mce.2025.112668.

Data availability

Data will be made available on request.

References

Allen-Brady, K., Moore, B., Verrilli, L.E., Alvord, M.A., Kern, M., Camp, N., Kelley, K., Letourneau, J., Cannon-Albright, L., Yandell, M., Johnstone, E.B., Welt, C.K., 2025. Breast cancer is increased in women with primary ovarian insufficiency. J. Clin. Endocrinol. Metab. 110, e1678–e1686. https://doi.org/10.1210/clinem/dgae480.

Amin, M., Horst, N., Wu, R., Gragnoli, C., 2023. Oxytocin receptor (OXTR) is a risk gene for polycystic ovarian syndrome. Eur. Rev. Med. Pharmacol. Sci. 27, 2634–2639. https://doi.org/10.26355/eurrev_202303_31800.

Azziz, R., Carmina, E., Chen, Z., Dunaif, A., Laven, J.S.E., Legro, R.S., Lizneva, D., Natterson-Horowtiz, B., Teede, H.J., Yildiz, B.O., 2016. Polycystic ovary syndrome. Nat. Rev. Dis. Primers 2. https://doi.org/10.1038/nrdp.2016.57.

B, L., W, C., X, Q., C, Y., Y, P., 2024. Interleukin-22 improves ovulation in polycystic ovary syndrome via STAT3 signaling. Mol. Hum. Reprod. 30. https://doi.org/10.1093/molehr/gaae037.

Bao, X., San, M., Wang, S., Zhuo, Y., Liu, Z., Zheng, Y., Li, D., 2025. Oxytocin receptor enhances adipocyte browning and energy metabolism in mice. Exp. Cell Res. 447, 114534. https://doi.org/10.1016/j.yexcr.2025.114534.

Burger, H.G., 2002. Androgen production in women. Fertil. Steril. 77 (Suppl. 4), S3–S5. https://doi.org/10.1016/s0015-0282(02)02985-0.

C, Z., J, M., W, W., Y, S., K, S., 2018. Lysyl oxidase blockade ameliorates anovulation in polycystic ovary syndrome. Hum. Reprod. Oxf. Engl. 33. https://doi.org/10.1093/humrep/dey292.

Cj, G., N, G., 2019. Characteristics of obesity in polycystic ovary syndrome: etiology, treatment, and genetics. Metabolism 92. https://doi.org/10.1016/j.metabol.2018.11.002.

Diamanti-Kandarakis, E., Piperi, C., Kalofoutis, A., Creatsas, G., 2005. Increased levels of serum advanced glycation end-products in women with polycystic ovary syndrome. Clin. Endocrinol. 62, 37–43. https://doi.org/10.1111/j.1365-2265.2004.02170.x.

Dumesic, D.A., Oberfield, S.E., Stener-Victorin, E., Marshall, J.C., Laven, J.S., Legro, R.S., 2015. Scientific statement on the diagnostic criteria, epidemiology, pathophysiology, and molecular genetics of polycystic ovary syndrome. Endocr. Rev. 36, 487–525. https://doi.org/10.1210/er.2015-1018.

Edinoff, A.N., Silverblatt, N.S., Vervaeke, H.E., Horton, C.C., Girma, E., Kaye, A.D., Kaye, A., Kaye, J.S., Garcia, A.J., Neuchat, E.E., Eubanks, T.N., Varrassi, G., Viswanath, O., Urits, I., 2021. Hyperprolactinemia, clinical considerations, and infertility in women on antipsychotic medications. Psychopharmacol. Bull. 51, 131–148.

Fauser, B.C.J.M., Tarlatzis, B.C., Rebar, R.W., Legro, R.S., Balen, A.H., Lobo, R., Carmina, E., Chang, J., Yildiz, B.O., Laven, J.S.E., Boivin, J., Petraglia, F., Wijeyeratne, C.N., Norman, R.J., Dunaif, A., Franks, S., Wild, R.A., Dumesic, D., Barnhart, K., 2012. Consensus on women's health aspects of polycystic ovary syndrome (PCOS): the amsterdam ESHRE/ASRM-sponsored 3rd PCOS consensus workshop group. Fertil. Steril. 97, 28–38.e25. https://doi.org/10.1016/j.fertnstert.2011.09.024.

Fuchs, A.R., Fields, M.J., Freidman, S., Shemesh, M., Ivell, R., 1995. Oxytocin and the timing of parturition. Influence of oxytocin receptor gene expression, oxytocin secretion, and oxytocin-induced prostaglandin F2 alpha and E2 release. Adv. Exp. Med. Biol. 395, 405–420.

Gimpl, G., Fahrenholz, F., 2001. The oxytocin receptor system: structure, function, and regulation. Physiol. Rev. 81, 629–683. https://doi.org/10.1152/physrev.2001.81.2.629.

Goodarzi, M.O., Azziz, R., 2006. Diagnosis, epidemiology, and genetics of the polycystic ovary syndrome. Best Pract. Res. Clin. Endocrinol. Metabol. 20, 193–205. https://doi.org/10.1016/j.beem.2006.02.005.

Hasan, R., 2024. The multifaceted role of oxytocinergic system and OXTR gene. Glob. Med. Genet. 11, 29–33. https://doi.org/10.1055/s-0044-1779039.

Hidema, S., Fukuda, T., Hiraoka, Y., Mizukami, H., Hayashi, R., Otsuka, A., Suzuki, S., Miyazaki, S., Nishimori, K., 2016. Generation of oxtr cDNA(HA)-ires-cre mice for gene expression in an oxytocin receptor specific manner. J. Cell. Biochem. 117, 1099–1111. https://doi.org/10.1002/jcb.25393.

Iovino, M., Messana, T., Tortora, A., Giusti, C., Lisco, G., Giagulli, V.A., Guastamacchia, E., De Pergola, G., Triggiani, V., 2021. Oxytocin signaling pathway: from cell biology to clinical implications. Endocr., Metab. Immune Disord.: Drug Targets 21, 91–110. https://doi.org/10.2174/1871530320666200520093730.

Jx, P., Yj, T., Ff, W., Nn, H., Yq, X., Jy, Z., Y, L., F, Q., Q, M., J, X., Jz, S., Hf, H., 2018. Aberrant expression and DNA methylation of lipid metabolism genes in PCOS: a new insight into its pathogenesis. Clin. Epigenet. 10. https://doi.org/10.1186/s13148-018-0442-y.

Kasahara, Y., Sato, K., Takayanagi, Y., Mizukami, H., Ozawa, K., Hidema, S., So, K.-H., Kawada, T., Inoue, N., Ikeda, I., Roh, S.-G., Itoi, K., Nishimori, K., 2013. Oxytocin receptor in the hypothalamus is sufficient to rescue normal thermoregulatory function in male oxytocin receptor knockout mice. Endocrinology 154, 4305–4315. https://doi.org/10.1210/en.2012-2206.

Kosfeld, M., Heinrichs, M., Zak, P.J., Fischbacher, U., Fehr, E., 2005. Oxytocin increases trust in humans. Nature 435, 673–676. https://doi.org/10.1038/nature03701.

L, M., R, H., S, F., A, J., M, J., 2023. Prolactin in polycystic ovary syndrome: Metabolic effects and therapeutic prospects. Life Basel Switz 13. https://doi.org/10.3390/life13112124.

L, S., X, H., W, L., 2025. Effects of liraglutide on leptin promoter methylation in ovarian granulosa cells of obese polycystic ovary syndrome patients. Tohoku J. Exp. Med. 266. https://doi.org/10.1620/tjem.2025.J009.

Li, R., Zhang, Q., Yang, D., Li, S., Lu, S., Wu, X., Wei, Z., Song, X., Wang, X., Fu, S., Lin, J., Zhu, Y., Jiang, Y., Feng, H.L., Qiao, J., 2013. Prevalence of polycystic ovary syndrome in women in China: a large community-based study. Hum. Reprod. Oxf. Engl. 28, 2562–2569. https://doi.org/10.1093/humrep/det262.

Li, D., Ji, Y., Zhao, C., Yao, Y., Yang, A., Jin, H., Chen, Y., San, M., Zhang, J., Zhang, M., Zhang, L., Feng, X., Zheng, Y., 2018. OXTR overexpression leads to abnormal mammary gland development in mice. J. Endocrinol. 239, 121–136. https://doi.org/10.1530/JOE-18-0356.

Li, D., San, M., Zhang, J., Yang, A., Xie, W., Chen, Y., Lu, X., Zhang, Y., Zhao, M., Feng, X., Zheng, Y., 2021. Oxytocin receptor induces mammary tumorigenesis through prolactin/p-STAT5 pathway. Cell Death Dis. 12, 588. https://doi.org/10.1038/s41419-021-03849-8.

Lim, C.P., Phan, T.-T., Lim, I.J., Cao, X., 2006. Stat3 contributes to keloid pathogenesis via promoting collagen production, cell proliferation and migration. Oncogene 25, 5416–5425. https://doi.org/10.1038/sj.onc.1209531.

Liu, S., Zeng, Q., Hu, L., Zeng, B., Wu, Y., Wang, C., Zhou, M., Gan, X., 2025. Recurrent giant ovarian cysts in biological sisters: 2 case reports and literature review-giant ovarian cysts in 2 sisters. Healthc. Basel Switz. 13, 656. https://doi.org/10.3390/healthcare13060656.

M, S., P, B., 2025. Ovulation induction techniques [WWW Document]. Pubmed. URL. https://pubmed.ncbi.nlm.nih.gov/34662078/. (Accessed 26 July 2025).

Ma, G., V, V., Ia, W., Ms, B., T, A., A, R., 2019. Epidemiology, pathogenesis, genetics & management of polycystic ovary syndrome in India. Indian J. Med. Res. 150. https://doi.org/10.4103/ijmr.IJMR_1937_17.

Malumbres, M., Mangues, R., Ferrer, N., Lu, S., Pellicer, A., 1997. Isolation of high molecular weight DNA for reliable genotyping of transgenic mice. Biotechniques 22, 1114–1119. https://doi.org/10.2144/97226st03.

Marshall, P.N., Horobin, R.W., 1973. The mechanism of action of "mordant" dyes–a study using preformed metal complexes. Histochem. Histochem. Histochim. 35, 361–371. https://doi.org/10.1007/BF00310675.

Mimouni, N.E.H., Paiva, I., Barbotin, A.-L., Timzoura, F.E., Plassard, D., Le Gras, S., Ternier, G., Pigny, P., Catteau-Jonard, S., Simon, V., Prevot, V., Boutillier, A.-L., Giacobini, P., 2021. Polycystic ovary syndrome is transmitted via a transgenerational epigenetic process. Cell Metab. 33, 513–530.e8. https://doi.org/10.1016/j.cmet.2021.01.004.

Naz, F., Malik, A., Riaz, M., Mahmood, Q., Mehmood, M.H., Rasool, G., Mahmood, Z., Abbas, M., 2022. Bromocriptine therapy: review of mechanism of action, safety and tolerability. Clin. Exp. Pharmacol. Physiol. 49, 903–922. https://doi.org/10.1111/1440-1681.13678.

Neumann, I.D., 2002. Involvement of the brain oxytocin system in stress coping: interactions with the hypothalamo-pituitary-adrenal axis. Prog. Brain Res. 139, 147–162. https://doi.org/10.1016/s0079-6123(02)39014-9.

Russell, J.A., Leng, G., Douglas, A.J., 2003. The magnocellular oxytocin system, the fount of maternity: adaptations in pregnancy. Front. Neuroendocrinol. 24, 27–61. https://doi.org/10.1016/s0091-3022(02)00104-8.

S, T., S, M., M, M., A, C., 2013. Induction of ovulation with clomiphene citrate versus clomiphene with bromocriptine in PCOS patients with normal prolactin: a comparative study. J. Clin. Diagn. Res. JCDR 7. https://doi.org/10.7860/JCDR/2013/7617.3605.

T, T., C, O., Gs, C., 2004. The pathophysiology of polycystic ovary syndrome. Clin. Endocrinol. 60. https://doi.org/10.1046/j.1365-2265.2003.01842.x.

T, G., J, O., P, K., R, K., R, M., M, B., M, H., 2024. Changes in prolactin and insulin resistance in PCOS patients undergoing metformin treatment: a retrospective study. J. Clin. Med. 13. https://doi.org/10.3390/jcm13247781.

Takayanagi, Y., Yoshida, M., Bielsky, I.F., Ross, H.E., Kawamata, M., Onaka, T., Yanagisawa, T., Kimura, T., Matzuk, M.M., Young, L.J., Nishimori, K., 2005. Pervasive social deficits, but normal parturition, in oxytocin receptor-deficient mice. Proc. Natl. Acad. Sci. U. S. A 102, 16096–16101. https://doi.org/10.1073/pnas.0505312102.

Ub, K., 2012. Hyperprolactinemia and infertility: new insights. J. Clin. Investig. 122. https://doi.org/10.1172/jci64455.

V, Y., T, S., 2025. Abnormally increased prolactin levels in women with polycystic ovarian syndrome are associated with risk of obesity, insulin resistance and prediabetes. Int. J. Mol. Sci. 26. https://doi.org/10.3390/ijms26094239.

V, K., Ud, G., A, L.B., 2016. Luteinizing hormone/chorionic gonadotrophin receptor overexpressed in granulosa cells from polycystic ovary syndrome ovaries is functionally active. Reprod. Biomed. Online 32. https://doi.org/10.1016/j.rbmo.2016.03.003.

Vale-Fernandes, E., Carrageta, D.F., Moreira, M.V., Guerra-Carvalho, B., Rodrigues, B., Sousa, D., Brandão, R., Leal, C., Barreiro, M., Tomé, A., Alves, M.G., Oliveira, P.F., Monteiro, M.P., 2025a. Follicular fluid profiling unveils anti-müllerian hormone alongside glycolytic and mitochondrial dysfunction as markers of polycystic ovary syndrome. Mol. Cell. Endocrinol. 602, 112536. https://doi.org/10.1016/j.mce.2025.112536.

Vale-Fernandes, E., Moreira, M.V., Bernardino, R.L., Sousa, D., Brandão, R., Leal, C., Barreiro, M., Monteiro, M.P., 2025b. Polycystic ovary syndrome and excessive body weight impact independently and synergically on fertility treatment outcomes. Reprod. Biol. Endocrinol. RBE 23, 97. https://doi.org/10.1186/s12958-025-01434-8.

Vale-Fernandes, E., Pignatelli, D., Monteiro, M.P., 2025c. Should anti-müllerian hormone be a diagnosis criterion for polycystic ovary syndrome? An in-depth review of pros and cons. Eur. J. Endocrinol. 192, R29–R43. https://doi.org/10.1093/ejendo/lvaf062.

Vaupel, P., Schmidberger, H., Mayer, A., 2019. The warburg effect: essential part of metabolic reprogramming and central contributor to cancer progression. Int. J. Radiat. Biol. 95, 912–919. https://doi.org/10.1080/09553002.2019.1589653.

W, C., Y, P., 2021. Metabolic syndrome and PCOS: pathogenesis and the role of metabolites. Metabolites 11. https://doi.org/10.3390/metabo11120869.

W, C., B, L., C, Y., M, Z., Y, P., 2024. Interlukin-22 improves ovarian function in polycystic ovary syndrome independent of metabolic regulation: a mouse-based experimental study. J. Ovarian Res. 17. https://doi.org/10.1186/s13048-024-01428-x.

X, Q., C, Y., L, S., J, X., Q, W., Y, W., L, W.Y., Zhang, X.L., L, W., Fj, G., Ad, P., H, L., L, M., Z, Z.Y., Zhao, R.L., P, L., C, Z., Y, P., C, J., J, Q., 2019. Gut microbiota-bile acid-interleukin-22 axis orchestrates polycystic ovary syndrome. Nat. Med. 25. https://doi.org/10.1038/s41591-019-0509-0.

Yq, F., Hk, Z., Qq, W., Yh, L., 2024. Brown adipose tissue-derived exosomes improve polycystic ovary syndrome in mice via STAT3/GPX4 signaling pathway. FASEB J. Off. Publ. Fed. Am. Soc. Exp. Biol. 38. https://doi.org/10.1096/fj.202401346R.

Zhang, Z., Jia, G., Wang, Q., Yu, Y., Tang, X., Zheng, H., Yang, X., Xiao, Y., Ou, Y., Jiang, J., Guo, H., Wang, Y., Li, S., 2025. Atherosclerosis enhances the efficacy of liposome-encapsulated bromocriptine in reducing the incidence of prolactinemia in pituitary tumors. J. Nanobiotechnol. 23, 392. https://doi.org/10.1186/s12951-025-03465-0.